Coupling between dynamic 3D tissue architecture and BMP morphogen signaling during *Drosophila* wing morphogenesis

Jinghua Gui[a,1], Yunxian Huang[a,2], Martin Montanari[a,2], Daniel Toddie-Moore[a], Kenji Kikushima[a], Stephanie Nix[b], Yukitaka Ishimoto[b], and Osamu Shimmi[a,3]

[a]Institute of Biotechnology, University of Helsinki, 00014 Helsinki, Finland; and [b]Department of Machine Intelligence and Systems Engineering, Akita Prefectural University, 015–0055 Akita, Japan

Edited by Norbert Perrimon, Harvard Medical School, Boston, MA, and approved January 17, 2019 (received for review September 7, 2018)

At the level of organ formation, tissue morphogenesis drives developmental processes in animals, often involving the rearrangement of two-dimensional (2D) structures into more complex three-dimensional (3D) tissues. These processes can be directed by growth factor signaling pathways. However, little is known about how such morphological changes affect the spatiotemporal distribution of growth factor signaling. Here, using the *Drosophila* pupal wing, we address how decapentaplegic (Dpp)/bone morphogenetic protein (BMP) signaling and 3D wing morphogenesis are coordinated. Dpp, expressed in the longitudinal veins (LVs) of the pupal wing, initially diffuses laterally within both dorsal and ventral wing epithelia during the inflation stage to regulate cell proliferation. Dpp localization is then refined to the LVs within each epithelial plane, but with active interplanar signaling for vein patterning/differentiation, as the two epithelia appose. Our data further suggest that the 3D architecture of the wing epithelia and the spatial distribution of BMP signaling are tightly coupled, revealing that 3D morphogenesis is an emergent property of the interactions between extracellular signaling and tissue shape changes.

epithelial morphogenesis | three-dimensional architecture | bone morphogenetic protein | drosophila | live-imaging

Formation of complex 3D tissues from simpler 2D precursors is a basic theme in animal development that often involves epithelial morphogenesis. Evolutionarily conserved growth factor signaling frequently contributes to these processes. Although how the cellular mechanisms of developmental signaling affect cell and tissue shapes has been actively studied, much less is known about how signaling and dynamic morphogenesis are mutually coordinated (1). Recent advances have indicated how morphogenesis and signaling can be coupled; for example, epithelial structures such as a lumen or villus can regulate the distribution of signaling factors to alter pathway activity (2–4). However, it remains to be addressed how the dynamic 3D tissue architecture affects developmental signaling in a precise spatiotemporal manner.

In *Drosophila*, wing development is a classical model in tissue morphogenesis. The larval wing imaginal disc has been used as a model to address the molecular mechanisms underlying tissue proliferation and patterning. Decapentaplegic (Dpp), a bone morphogenetic protein (BMP) 2/4 type-ligand and member of the TGF-β family of signaling molecules, has been implicated in regulating a diverse array of developmental events, including wing disc development (5). During the larval stage, *dpp* is transcribed in a stripe at the anterior/posterior compartment boundary of the wing imaginal disc, and Dpp forms a long-range morphogen gradient that regulates tissue size and patterning (6, 7). Dpp signaling is needed for tissue proliferation, and Dpp activity gradient formation is crucial for patterning during the late third instar larval stage (8, 9). These processes largely take place within a 2D space, the single cell layer of the wing imaginal disc epithelium.

During the pupal stage that follows, the wing imaginal disc everts to become a two-layered, 3D wing composed of dorsal and ventral epithelial cells (10–13). Previous studies have suggested that pupal wing development is divided into three phases during the first day of pupal development (10, 14, 15). In the first phase, first apposition [0–10 h after pupariation (AP)], a single-layered wing epithelium everts and forms dorsal and ventral epithelia to become a rudimentary two-layered wing. In the next phase, inflation (10–20 h AP), the two epithelia physically separate before fusing in the third phase, second apposition, at around 20 h AP (Fig. 1*A* and Movie S1). Therefore, dynamic morphological changes in 3D architecture are taking place during the first 24 h AP, making this tissue an ideal model to investigate the changes in signaling molecule directionality as a more complex 3D tissue arises from a 2D precursor, and thus how 3D architecture and developmental signaling are coupled.

During pupal wing development, Dpp signaling is known to play a role in wing vein differentiation. This is largely based on analysis of the *shortvein* group of *dpp* alleles containing deficiencies at the 5′ locus that manifest in partial vein loss phenotypes in the adult wing (16, 17). In this study, we re-evaluated the function of Dpp signaling in pupal wing development. Our data reveal that during pupariation, Dpp signaling is needed not only for vein differentiation and patterning, but also has an unexpected key role in tissue proliferation. Specifically, Dpp

Significance

Tissue morphogenesis is a dynamic process often accompanied by cell patterning and differentiation. Although how conserved growth factor signaling affects cell and tissue shapes has been actively studied, much less is known about how signaling and dynamic morphogenesis are mutually coordinated. Our study shows that BMP signaling and 3D morphogenesis of the *Drosophila* pupal wing are tightly coupled. These findings are highlighted by the fact that the directionality of BMP signal is changed from lateral planar during the inflation stage to interplanar after re-apposition of the dorsal and ventral wing epithelia. We suspect that the dynamic interplay between planar and interplanar signaling linked to tissue shape changes is likely to be used across species in many developing organs.

Author contributions: J.G. and O.S. designed research; J.G., Y.H., M.M., D.T.-M., and O.S. performed research; K.K., S.N., and Y.I. contributed new reagents/analytic tools; J.G., Y.H., and O.S. analyzed data; and J.G., M.M., D.T.-M., and O.S. wrote the paper.

The authors declare no conflict of interest.

This article is a PNAS Direct Submission.

[1]Present address: Department of Genetics, University of Cambridge, United Kingdom.

[2]Y.H. and M.M. contributed equally to this work.

[3]To whom correspondence should be addressed. Email: osamu.shimmi@helsinki.fi.

This article contains supporting information online at www.pnas.org/lookup/suppl/doi:10.1073/pnas.1815427116/-/DCSupplemental.

Published online February 13, 2019.

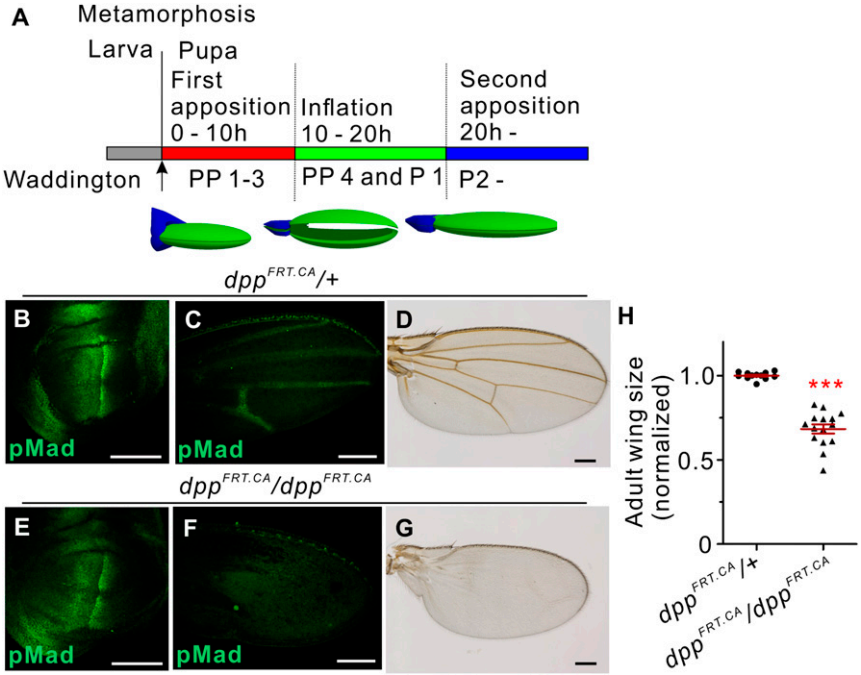

Fig. 1. Dpp/BMP signal regulates proliferation and patterning of the *Drosophila* pupal wing. (*A*) Timing of wing development during the first 24 h after pupariation at 25 °C. Pupal wing development is divided into three phases; first apposition (0–10 h AP), inflation (10–20 h AP), and second apposition (from 20 h onwards). Developmental stages [PP (prepupal) 1–4 and P (pupal) 1–2] described by C. H. Waddington are included (14). A schematic of each pupal stage is shown below (hinge in blue and wing in green). Size and tissue shape are not proportional to actual wings. (*B–D*) pMad staining pattern in wing disc (*B*), 24 h AP pupal wing (*C*) and an adult wing in control ($dpp^{FRT.CA}$/+) (*D*). (*E–G*) pMad staining pattern in wing disc (*E*), 24 h AP pupal wing (*F*), and an adult wing in dpp^{FO} ($dpp^{FRT.CA}/dpp^{FRT.CA}$) (*G*). (Scale bars: 100 μm for *B*, *C*, *E*, and *F*, and 200 μm for *D* and *G*.) (*H*) Size comparison between control and dpp^{FO} wings of adult wings. Means ± SEM, ***$P < 0.001$, two-paired *t* test with 95% confidence intervals (CIs). Larvae were reared at 18 °C and then transferred to 29 °C 8 h before pupariation, followed by dissecting wing imaginal discs (*B* and *E*), collecting at 24 h AP and dissecting pupal (*C* and *F*) or adult stage wings (*D* and *G*). Sample sizes: are $n = 12$ (control) and $n = 15$ (dpp^{FO}) in *H*.

expressed in the longitudinal veins (LVs) diffuses laterally to regulate tissue size during the inflation stage. Intriguingly, we find that as dorsal and ventral wing epithelia appose, the direction of Dpp signaling changes from lateral within each epithelium to interplanar between the epithelia. We presume that this results in refinement of Dpp signaling range in the vein regions, which in turn contributes to precise matching of vein patterning in dorsal and ventral epithelia. Dpp signaling directionality thus changes from 2D lateral planar to 3D interplanar. Our data further suggest that 3D tissue architecture directs the spatial distribution of Dpp/BMP signaling. These results provide new insights into the mechanism and regulation of 3D morphogenesis.

Results

Dpp/BMP Signal Regulates Proliferation and Patterning of the Pupal Wing. To re-evaluate the function of Dpp signaling in pupal wing development, we used conditional knockout approaches to remove *dpp* in a stage-specific manner. When the knockout was induced in the wing pouch of the wing imaginal disc 24 h before pupariation using a conditional *dpp* allele (8), we found that *dpp* expression was efficiently ablated in the pupal wing (*SI Appendix*, Fig. S1 *A* and *B*). Consistent with previous reports, late third instar wing imaginal discs were of equivalent sizes in control and *dpp* knockout animals 24 h after induction, even though anti-phosphoMad (pMad) antibody staining, a readout of BMP signaling, was diminished in the wing pouch (*SI Appendix*, Fig. S1 *C*, *F*, and *I*) (8). The BMP signal is also lost in *dpp* knockout wings. Intriguingly, pupal wing sizes of *dpp* knockout animals are significantly smaller than in controls at 24 h AP (*SI Appendix*, Fig. S1 *D*, *G*, and *J*). Consistent with this observation, adult wing sizes of *dpp* knockout animals are smaller than that of the control, and wing vein formation is largely abolished (*SI Appendix*, Fig. S1 *E*, *H*, and *K*). Recently, alternative conditional *dpp* knockout alleles have been developed (9), which provide more rapid gene inactivation. Using one of these alternative alleles, we found that BMP signaling was efficiently ablated in the pupal wing, but not in the larval wing imaginal disc, when *dpp* knockout was induced 8 h before pupariation (Fig. 1 *B*, *C*, *E*, and *F*). As shown with the previous knockout allele, these experiments resulted in significantly smaller size and loss of wing vein formation in adult wings compared with controls (Fig. 1 *D*, *G*, and *H*).

To verify independently that these phenotypes are caused by loss of Dpp/BMP signaling in the pupal wing, BMP signal was inhibited in a pupal stage-specific manner by overexpressing *Dad*, an inhibitory Smad (18), resulting both in reduced wing size and in loss of venation in adult wings (*SI Appendix*, Fig. S1 *L*, *N*, and *P*). pMad signaling is also lost in the vein primordia of the pupal wings (*SI Appendix*, Fig. S1 *M* and *O*). Taken together, these results indicate that the Dpp/BMP signal plays a crucial role in tissue growth and patterning in wing development during pupal stages.

Growth of the Pupal Wing Involves Dpp/BMP Signaling. Positing that Dpp/BMP signaling plays a role in tissue growth of the pupal wing, how is cell proliferation spatiotemporally regulated? Previous studies indicate that cell division in the pupal wing mainly takes place during the inflation stage, without however identifying the molecular mechanisms regulating cell proliferation (19–22). To address whether the Dpp/BMP signal regulates cell proliferation, phosphorylated-histone H3 (pH3) antibody staining was carried out at different time points to detect mitotic cells. The numbers of pH3-positive cells gradually decrease during 18–24 h

AP and are essentially zero at 26 h AP in wild-type wings (Fig. 2 *A*–*F*). The numbers of pH3-positive cells in *dpp* knockout wings are significantly lower than control during 18–20 h AP (Fig. 2 *G*–*J*), indicating that Dpp is required for normal proliferation.

Despite *dpp* expression previously being described only in the LVs (23), pH3-positive cells are frequently observed in the intervein region. One possibility is that a long-range Dpp signal is needed for cell proliferation during the inflation stage. To

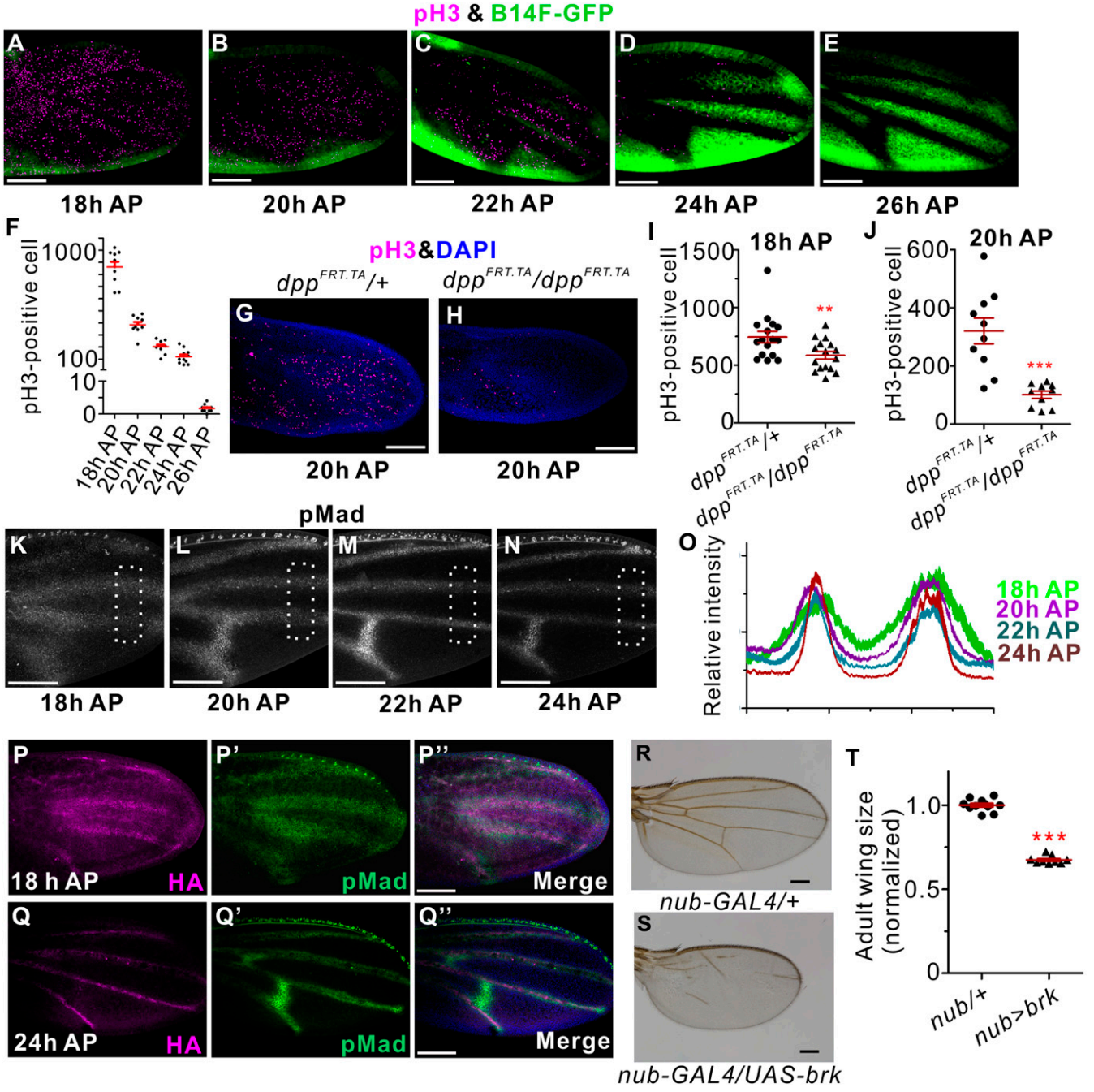

Fig. 2. Growth of the *Drosophila* pupal wing involves Dpp/BMP signaling. (*A*–*E*) pH3 staining (magenta) and *brk-GFP* (green) of pupal wings in brk^{B14F}*-GFP* in an otherwise wild-type background at 18 h (*A*), 20 h (*B*), 22 h (*C*), 24 h (*D*) and 26 h AP (*E*). (*F*) Numbers of pH3-positive cells in control at 18 h, 20 h, 22 h, 24 h and 26 h AP. Mean ± SEM (*G* and *H*) pH3 staining (magenta) and DAPI (blue) in control (*G*) and conditional knockout (*H*) at 20 h AP. (*I* and *J*) Numbers of pH3-positive cells in control ($dpp^{FRT.TA}$/+) and *dpp* conditional knockout ($dpp^{FRT.TA}/dpp^{FRT.TA}$) at 18 h (*I*) and 20 h AP (*J*). Mean ± SEM $^{**}P < 0.01$, $^{***}P < 0.001$, two-paired *t* test with 95% CIs. (*K*–*N*) pMad expression in the pupal wings in wild type at 18 h (*K*), 20 h (*L*), 22 h (*M*), and 24 h AP (*N*). (*O*) Plot profile analysis of pMad staining in ROIs in *K*–*N*, corresponding to 18 h, 20 h, 22 h and 24 h AP. Mean ± SEM, $n = 6$ for each. (*P* and *Q*) Anti-HA antibody staining in dpp^{HA}/+ animals at 18 h (*P*) and 24 h AP pupal wing (*Q*). pMad expression in the pupal wing (*P*′ and *Q*′). Merged images of anti-HA (magenta), pMad (green) and DAPI (blue) (*P*″ and *Q*″). (*R* and *S*) Adult wings in control (*R*) and *brk* overexpression during pupal stage (*S*). (Scale bars: 100 μm for *A*–*E*, *G*, *H*, *K*–*N*, *P*, and *Q*, and 200 μm for *R* and *S*.) (*T*) Size comparison between control and *brk* overexpression of adult wings. Larvae were reared at 18 °C and then transferred to 29 °C after having reached the prepupal stage. Mean ± SEM, $^{***}P < 0.001$, two-paired *t* test with 95% CIs. Sample sizes are 10 (18 h), 10 (20 h), 10 (22 h), 11 (24 h), 10 (26 h AP) in *F*, 16 (control) and 16 (dpp^{FO}) in *I*, 10 (control) and 10 (dpp^{FO}) in *L*, and 11 (control) and 9 (*brk* overexpression) in *T*.

investigate this, we examined *dpp* expression and Dpp/BMP signal activity during the inflation and second apposition stages. Similarly to wing imaginal discs, *dpp* is expressed at the anterior-posterior boundary in the early prepupal wing around 5 h AP (*SI Appendix*, Fig. S2*A*). Thereafter, expression gradually changes to the positions of future LVs, where it persists until the second apposition stage (*SI Appendix*, Fig. S2 *B–D*). We then measured Dpp/BMP signaling by using pMad antibody staining and *brinker (brk)-GFP* (a GFP reporter of the regulatory fragment B14 of *brk*) (24). Brk is a repressor of BMP signal in the wing tissue, expression of which is negatively regulated by BMP signaling (24–27). Our data reveal that the peak level of pMad staining is observed centered on the future LVs, and that lower pMad levels are spread throughout the intervein cells at 18 h AP (Fig. 2 *K* and *O*). *brk-GFP* expression is barely detected at the periphery of the pupal wing at 18 h AP, indicating that BMP signaling is occurring throughout the pupal wing (Fig. 2*A*) at this time point. When the Dpp/BMP signal was inhibited by overexpressing *Dad*, pMad expression is not detected, but *brk-GFP* is ubiquitously expressed in the pupal wing at 18 h AP (*SI Appendix*, Fig. S2 *E* and *E′*). To address how Dpp ligand is spatiotemporally regulated in the pupal wing, animals expressing HA-tagged Dpp under the control of the genomic *dpp* promoter were utilized (9). HA-Dpp is found not only in the future vein cells (that are ligand-producing cells), but also in intervein cells, at 18 h AP (Fig. 2 *P–P″*). Taken together, these results suggest that Dpp forms an activity gradient emanating from future LV cells during the inflation stage.

Intriguingly, the pattern of pH3-positive proliferating cells reflects patterns complementary to *brk* expression (Fig. 2 *A–E*). In larval wing imaginal discs, loss of *brk* appears to be sufficient for cell proliferation (28, 29). A recent study further suggests that low-level Dpp signaling (below the level needed for substantial pMad accumulation, but enough for repressing *brk* expression) is sufficient for tissue growth in the wing disc (9). Thus, we examined whether Brk is also a key regulator of proliferation in the pupal wing. Our data reveal that overexpression of *brk* in the wing pouch during the pupal stage results in significantly smaller wings than in the control, resembling our previous findings for loss-of-function of *dpp* in the pupal wing (Fig. 2 *R–T*). These results indicate that Dpp trafficking takes place laterally during the inflation stage, and controls cell proliferation by regulating *brk* expression.

As wing development progresses from inflation to second apposition, pMad staining gradually becomes refined to the cells of future LVs, and *brk-GFP* expression is progressively upregulated in the intervein regions (Fig. 2 *A–E* and *K–O*). Moreover, HA-Dpp is tightly localized at future vein cells (Fig. 2 *Q–Q″*). These results are consistent with previous reports that the Dpp/BMP signal is restricted to LVs at around 24 h AP (23). These data further suggest that while the wing tissue is undergoing 3D morphological modifications between the inflation and second apposition stages, the BMP signaling range and pattern are also undergoing dynamic changes.

Coordination of BMP Signaling and Patterning Between Dorsal and Ventral Epithelia of the Pupal Wing. What role does Dpp/BMP signaling play in the 3D regulation of growth and patterning in the dorsal and ventral epithelia? First, to understand dynamics of the 3D structure of the pupal wing, we obtained time-lapse images of optical cross sections of the pupal wing between 18 h and 24 h AP. These images indicate that maximum distances between dorsal and ventral epithelia are greater than 100 μm at 18 h AP, then gradually decrease during reapposition starting around 20 h AP, resulting in reapposed dorsal and ventral epithelia of the *Drosophila* wing matching in both size and patterning (i.e., vein and intervein cells) (Fig. 3 *A–F* and Movie S2). This raises the question of whether patterning and morphogenesis of the two epithelia are regulated independently, or in a coordinated manner. To address this, we next tested whether BMP signal transduction acts independently in dorsal and ventral layers during wing morphogenesis. When BMP signaling was reduced only in the dorsal wing epithelium during the pupal stage, by either overexpression of *Dad*, or by knockdown of BMP type-I receptor *thickveins* (*tkv*), adult wings were smaller than in control flies, and displayed partial disruption of vein formation (Fig. 3 *G–I* and *M*). BMP signal transduction was lost in the dorsal pupal wing as expected (Fig. 3 *J–L*). Intriguingly, pMad expression in the ventral epithelium was not refined, but instead remained broad at 24 h AP, even though the ventral cells are wild-type (Fig. 3 *J′–L′*). Furthermore, optical cross sections of the fixed tissues suggest that dorsal and ventral epithelia are not properly fused by 24 h AP (Fig. 3 *J″–L″*). Taken together, these results indicate that reducing Dpp signaling solely in one 2D epithelial layer alters the 3D structure of the pupal wing, reducing tissue size and changing patterning of the final adult wing.

We then induced a conditional knockout of *dpp* in the dorsal layer only during pupal stages. In control tissues, pMad expression, the downstream readout of Dpp signaling, shows a similar pattern in dorsal and ventral tissues at both 18 h and 24 h AP (*SI Appendix*, Fig. S3 *A* and *B*). In contrast, in the conditional *dpp* knockout tissues, pMad expression was only observed in the ventral cells at 18 h AP, and thereafter detected in the dorsal cells by 24 h AP (Fig. 3 *N* and *O*). Intriguingly, wing vein patterning in conditional knockout adult wings appears largely normal, but tissue size is significantly smaller than in control animals (Fig. 3 *P–R*), which is caused by significant reduction of the numbers of proliferating cells in both dorsal and ventral tissues (*SI Appendix*, Fig. S3 *C–E*). These results suggest that Dpp ligands expressed in the ventral epithelial layer can induce BMP signaling in the dorsal layer after reapposition to sustain wing vein development, but tissue proliferation during the inflation stage appears to require ligand production in both dorsal and ventral tissues.

Interplanar BMP Signaling Between Dorsal and Ventral Epithelia of the Pupal Wing. How then is Dpp/BMP signaling regulated between the two epithelial layers? To test whether Dpp is able to move between dorsal and ventral epithelia during the second apposition stage, we employed mosaic analysis with a repressible cell marker (MARCM) (30). When GFP:Dpp-expressing clones are induced in the intervein region of only one epithelial sheet, pMad expression is observed not only in these ligand-producing cells, but also in the opposite epithelium in a matching pattern at 24 h AP (Fig. 4 *A–D*). In contrast, pMad expression is only detected in the ligand-producing cells and the flanking regions of the clones, but not in the opposite layer, during wing inflation at 18 h AP (*SI Appendix*, Fig. S4 *A* and *B*), in support of the notion that Dpp signal transduction takes place vertically after reapposition. We previously reported that a positive feedback mechanism through BMP signaling is needed to maintain a short-range Dpp/BMP signal in LVs at 24 h AP (23). We next examined whether a positive feedback mechanism is also crucial for interplanar BMP signaling. When Dad was overexpressed in Dpp-expressing clones in the intervein region of only one epithelial sheet, pMad expression is observed mostly in the flanking regions of the clones in the same plane. In contrast, pMad is observed at the site of the clones in the opposite epithelial layer in both ligand expressing cells and flanking regions (*SI Appendix*, Fig. S4 *C* and *D*). These results suggest that lateral signaling in the same plane is tightly regulated by active retention through positive feedback mechanisms (23), and in contrast, vertical signaling between the two epithelia appears to be regulated by a distinct mechanism.

Coupling Between BMP Signaling and 3D Tissue Architecture. As we observed interplanar signaling between apposed epithelia at 24 h AP, but not during inflation at 18 h AP, one conjecture is that

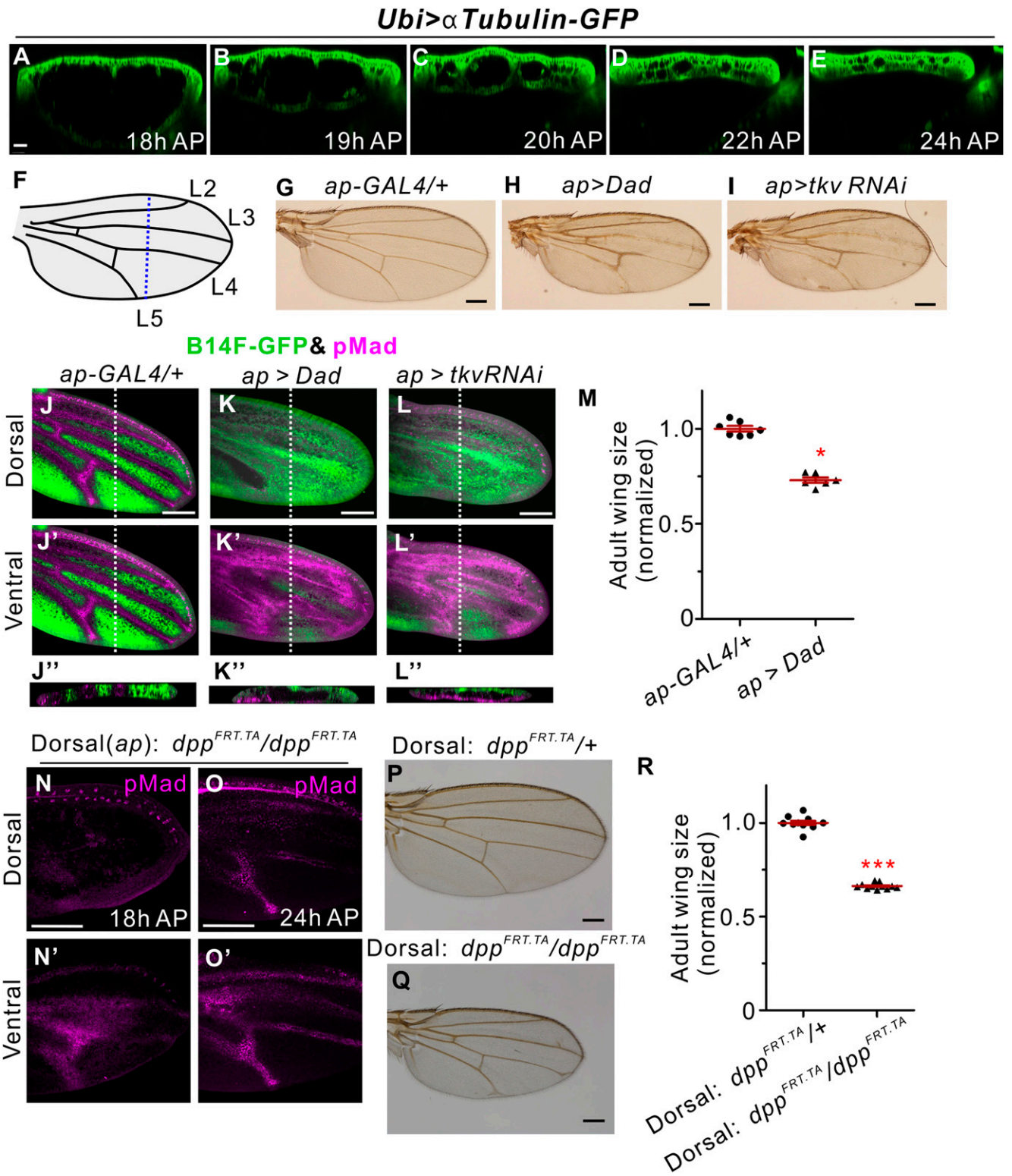

Fig. 3. Coordination of BMP signaling between dorsal and ventral epithelia of the pupal wing. (*A*–*E*) Time-lapse images of anteroposterior optical cross sections of αTubulin-GFP at 18 h (*A*), 19 h (*B*), 20 h (*C*), 22 h (*D*) and 24 h AP (*E*). Anterior is left and posterior right. Dorsal is up and ventral down. (*F*) Schematic of pupal wing. Approximate position of imaging in *A*–*E* is shown as a dotted line. (*G*–*I*) Control (*G*), *Dad* overexpression (*H*), and *tkv* knockdown adult wings (*I*). (*J*–*L*) pMad expression (magenta) and *brk-GFP* (green) of dorsal (*J*–*L*) and ventral tissues (*J*′–*L*′) in control (*J*), *Dad* overexpression (*K*), and *tkv* knockdown (*L*) at 24 h AP. Optical cross sections focused on the area shown by dotted lines (*J*″–*L*″). Dorsal aspect is up, and ventral down. (*M*) Size comparison between control and *Dad* overexpression adult wings. Larvae were reared at 18 °C and then transferred to 29 °C after having reached the prepupal stage. Mean ± SEM $*P < 0.05$, two-paired *t* test with 95% CIs. (*N* and *O*) pMad expression in dorsal (*N* and *O*) and ventral epithelia (*N*′ and *O*′) in *ap* > dpp^{FO} at 18 h (*N*), and at 24 h AP (*O*). (*P* and *Q*) adult wings in control (*P*) and *ap* > dpp^{FO} (*Q*). (Scale bars: 20 μm for *A*, 200 μm for *G*–*I*, *P*, and *Q*, and 100 μm for *J*–*L*, *N*, and *O*.) (*R*) Size comparison between control and *ap* > dpp^{FO} adult wings. Larvae were reared at 18 °C and then transferred to 29 °C 24 h before pupariation, followed by collecting at 18 h (*N*) and 24 h AP (*O*) and dissecting pupal or adult wings (*P* and *Q*). Mean ± SEM $***P < 0.001$, two-paired *t* test with 95% CIs. Sample sizes are 7 (control) and 6 (*Dad* overexpression) in *M*, and 11 (control) and 11 (*ap* > dpp^{FO}) in *R*.

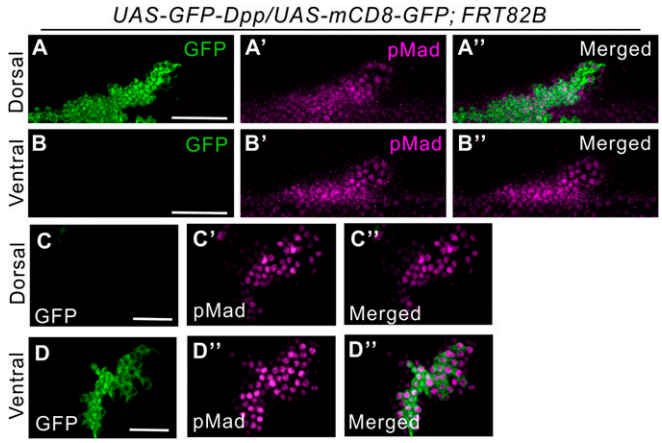

Fig. 4. Interplanar BMP signaling between dorsal and ventral epithelia of the pupal wing. (*A–D*) Dorsal (*A* and *C*) and ventral (*B* and *D*) epithelia of the pupal wings expressing GFP-Dpp clones in dorsal layer (green, *A* and *B*) or ventral layer (green, *C* and *D*) at 24 h AP. pMad expression (magenta, *A′–D′*). Merged images (*A″–D″*). (Scale bars: 20 μm.)

the distance between dorsal and ventral tissues may be a crucial factor in interplanar signaling. The 3D architecture of the developing pupal wing rapidly changes during inflation and second apposition stages (Fig. 3 *A–E* and Movie S2). Therefore, we assessed relationships between BMP signaling and 3D architecture of the pupal wing using live time-lapse imaging. Since refinement of BMP signaling can be traced by *brk* expression, we used Brk-GFP flies to obtain time-lapse images of optical cross sections of the pupal wing between 18 h and 26 h AP. RFP-labeled histone H2Av was used to monitor the position of individual cell nuclei (31). Similarly to fixed tissues (Fig. 2 *A–E*), Brk-GFP is observed after 20 h AP in intervein cells (Fig. 5 *A–F*, *SI Appendix*, Fig. S5 *A–F*, and Movie S3). Importantly, the gap between dorsal and ventral tissues begins to close before *brk* expression is observed. If refinement of BMP signaling in wing vein progenitor cells and 3D tissue architecture are coupled, we expect that 3D tissue dynamics may change when BMP signaling is manipulated. Our data in fixed tissues indicate that 3D architecture is different from control at 24 h AP when BMP signaling is disrupted in the dorsal tissues (Fig. 3 *K″* and *L″*). To confirm this, we performed live imaging of pupal wings overexpressing Dad in dorsal epithelium. We obtained time-lapse images of optical cross sections of the pupal wing between 18 h and 26 h AP (Fig. 5 *G–L*, *SI Appendix*, Fig. S5 *G–L*, and Movie S4). Apposition of dorsal and ventral epithelia is significantly delayed, and consequently, Brk-GFP is ubiquitously expressed in the dorsal tissues and less induced in the ventral cells at 24 h AP, than in control (Fig. 5 *G–L*, *SI Appendix*, Fig. S5 *G–L*, and Movie S4). These results suggest that the 3D architecture of the pupal wing and spatial distribution of BMP signaling are tightly coupled.

3D Architecture of the Pupal Wing Instructs Spatial Distribution of BMP Signaling. We next hypothesized that the 3D architecture of wing morphogenesis may be a key regulator of Dpp signaling. To test this idea, we sought to artificially modulate the 3D structure by gently squeezing the pupal abdomen at around 18 h AP (Fig. 6*A* and Movies S5 and S6). This resulted in excess flow of hemolymph into the wing interepithelial space, causing an increased distance between dorsal and ventral epithelia compared with control animals at 22 h AP, and thus extending the inflation stage. Surprisingly, in wings of squeezed pupae, pMad expression is not refined in sharp stripes, and *brk* expression is less induced in the intervein region at 22 h AP (Fig. 6 *B* and *C*). Consequently, the proliferation phase appears to last longer, as indicated by more pH3-positive cells at 22 h AP than in controls (Fig. 6 *B* and *D*). Importantly, cellular distribution of HA-Dpp is altered with abdominal squeezing. In control tissues, HA-Dpp is highly localized in the future vein cells at basolateral domains (Fig. 6*E*). In contrast, HA-Dpp is dispersed throughout intervein cells in squeezed 24 h AP pupal wings (Fig. 6*F*), suggesting that change of 3D architecture affects spatial regulation of Dpp ligands. We also noticed that Tkv distribution, shown by expression of Tkv:YFP, is affected by abdominal squeezing (Fig. 6*C*). Since Tkv levels have been proposed to be a key component in Dpp distribution (32), this further suggests how dynamic changes in 3D tissue structure affect signaling distribution. The effects we observe on HA-Dpp and Tkv:YFP distribution are unlikely to arise due to globally delayed development in abdominally squeezed animals, as both squeezed animals and unsqueezed controls develop into adults in a similar time frame (*SI Appendix*, Fig. S6). Taken together, these results indicate that 3D architecture of the pupal wing instructs how the Dpp signal is regulated during the processes of tissue proliferation and patterning/differentiation.

Discussion

We use the *Drosophila* pupal wing as a model to understand how 3D morphogenesis of an entire tissue and developmental signaling are coordinated. Although the *Drosophila* pupal wing has not historically been a widely acknowledged model of 3D tissue architecture formation, the dynamic 3D structure in pupal wing development has been described previously (14), and communication between dorsal and ventral epithelia has also been postulated (33). We propose that the *Drosophila* pupal wing serves as an excellent model for 3D morphogenesis for the following reasons: First, the dynamics of 3D architecture of the pupal wing are observed in a relatively short time period, with three distinct stages, and both structural changes and signaling outputs are easily tracked at the cellular level. Second, time-lapse imaging techniques enable us to observe straightforwardly the dynamics of 3D tissue architecture and signaling, and to investigate in real time how morphological changes and signaling are coupled. Third, by using a protocol developed in this study, 3D architecture of the pupal wing can be manipulated

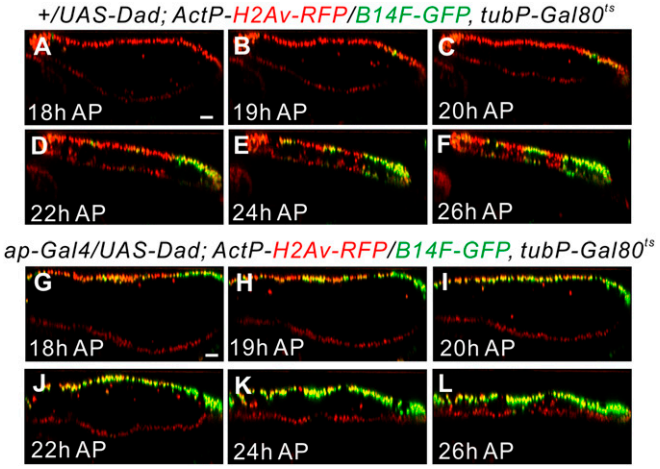

Fig. 5. Coupling between BMP signaling and 3D tissue architecture. (*A–F*) Time-lapse images of anteroposterior optical cross sections in *HistoneH2Av-RFP*, *brk^{B14F}-GFP* in pupal wing at 18 h (*A*), 19 h (*B*), 20 h (*C*), 22 h (*D*) 24 h (*E*) and 26 h AP (*F*). (*G–J*) Time-lapse images of anteroposterior optical cross sections of *HistoneH2Av-RFP*, *brk^{B14F}-GFP* in Dad overexpression in the dorsal epithelium in pupal wing at 18 h (*G*), 19 h (*H*), 20 h (*I*), 22 h (*J*) 24 h (*K*) and 26 h AP (*L*). (Scale bars: 20 μm.) Anterior is left and posterior right. Dorsal is up and ventral down.

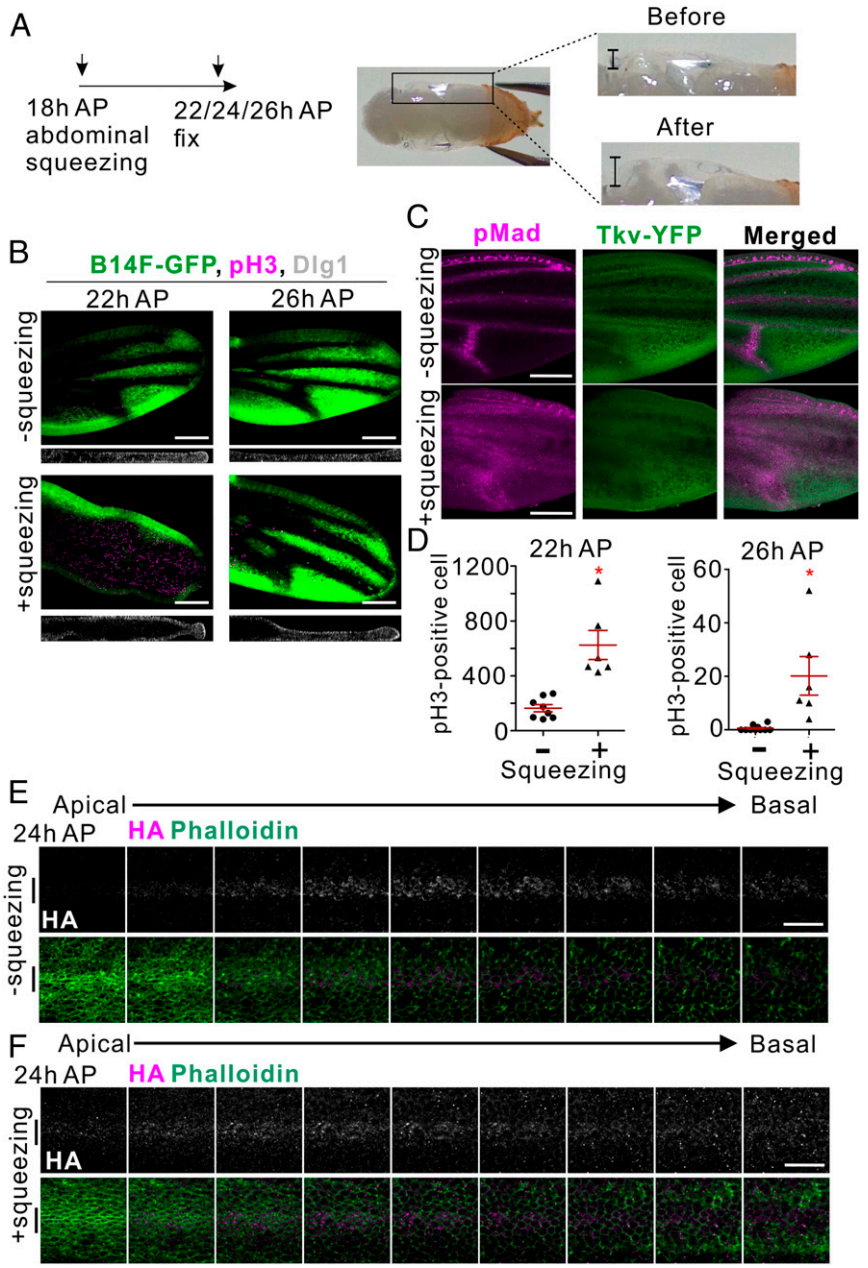

Fig. 6. 3D architecture of the pupal wing instructs spatial distribution of BMP signaling. (*A*) Schematic of abdominal squeezing at 18 h AP. Pupal tissues were fixed at indicated stages for experiments. Tissue architecture of pupal wings is artificially manipulated through abdominal squeezing (*Right*). Note that inflation between dorsal and ventral epithelia (bars) (wing 3D architecture) is exaggerated after squeezing. (*B*) *brk-GFP* expression (green) and pH3 staining (magenta) in pupal wings with or without squeezing at 22 h and 26 h AP. Optical cross sections of the DLG1-stained pupal wings (basolateral staining in wing epithelial cells) are shown in the *Lower* panels. (*C*) pMad expression (magenta) and Tkv-YFP (green) in pupal wings with or without squeezing at 22 h AP. (*D*) Numbers of pH3-positive cells in pupal wings with or without squeezing at 22 h and 26 h AP. Mean ± SEM **P* < 0.005, two-paired *t* test with 95% CIs. Sample sizes are 8 (no squeezing) and 6 (squeezing) at 22 h AP, and 10 (no squeezing) and 6 (squeezing) at 26 h AP in *D*. (*E* and *F*, *Upper*) Anti-HA antibody staining in pupal wings of dpp^{HA}/+ without squeezing (*E*) or with squeezing (*F*) at 24 h AP. (*E* and *F*, *Lower*) Merged images of anti-HA (magenta) and phalloidin (green). Snapshots of nine different sections of the cells covering L3 along the apicobasal axis at a 1-μm interval. Bars to left of panels show the position of ligand producing cells (future longitudinal vein cells). (Scale bars: 100 μm for *B* and *C*, and 20 μm for *E* and *F*.)

without genetic and developmental timing changes (Fig. 6, *SI Appendix*, Fig. S6, and Movies S5 and S6). This allows us to investigate experimentally how the assumption of 3D tissue architecture involves spatiotemporal regulation of developmental signaling.

Dpp morphogen signaling in the larval wing imaginal disc has been actively studied as a 2D model (6, 7). Recent studies suggest that Dpp signaling impacts both proliferation and patterning in distinct manners. One study proposes that early stage Dpp signaling is sufficient for tissue proliferation, and the Dpp morphogen gradient at the third instar larval stage is needed for patterning (8). In contrast, a separate study suggests that Dpp signal is needed for proliferation during the third larval instar, at least at a level sufficient to down-regulate *brk* expression (9). In this study, our data suggest that Dpp signaling is required after the third larval instar in the pupal wing for cell proliferation and

wing vein patterning/differentiation. This is further highlighted by the fact that these processes are likely affected by the observed changes in Dpp signaling directionality. During the inflation stage, active Dpp trafficking takes place laterally from future LV regions to spread BMP signal throughout the tissue. The pMad staining pattern indicates BMP activity gradient formation centered on LVs (that are ligand producing cells) at 18 h AP (Fig. 2). It is likely that the proliferation rate during pupal wing development is a critical factor to determine final tissue size in the adult. Our data clearly reveal that loss of BMP signal results in reduction of proliferation rate, leading to smaller adult tissue size. As development progresses from inflation to second apposition, both the pMad staining pattern and *brk* expression reveal that the BMP signaling range becomes refined (Fig. 2). Strikingly, BMP signal transduction actively takes place between dorsal and ventral epithelia (Figs. 3 and 4), which may play a role in refinement of the signaling range. These findings suggest that the dynamic interplay between planar and interplanar signaling is linked to coordinate tissue size and patterning.

One of the interesting observations in this study is that when *dpp* expression was ablated only in dorsal cells, tissue size is smaller than control, but overall patterning appears mostly normal (Fig. 3 *P*–*R*). These data clearly support our postulation that Dpp regulates proliferation and patterning/differentiation in distinct manners during pupal wing development. Furthermore, tissue size between dorsal and ventral layers appears to be coordinated when growth signal in only one of the epithelia is manipulated, suggesting the existence of hitherto unidentified mechanisms that coordinate mitosis between dorsal and ventral epithelial cells. Combined with previous studies about Dpp signaling affecting growth and patterning in the larval wing imaginal disc, our data reveal co-optation of the Dpp signaling pathway in the transition from a 2D anlage to a 3D organ.

Our key claim in this work is that formation of 3D tissue architecture and Dpp signaling are tightly coupled (Fig. 7). We support our claim by the following experimental observations. First, the spatiotemporal distribution of Dpp ligand and 3D tissue architecture are mutually coordinated. Our data reveal that Dpp ligand distribution changes during inflation and second apposition stages (Figs. 2, 4, and 7). Importantly, spatial cellular regulation of Dpp ligand appears to be under control of 3D tissue architecture (Figs. 5 and 6). Second, interplanar signaling between dorsal and ventral cells depends on the distance between the two epithelia. Our live-imaging of the pupal wing (Fig. 5) supports this claim. This has been further corroborated by changing the 3D architecture of the pupal wing using the abdominal squeezing technique we developed (Fig. 6). Importantly, this method simply changes the 3D tissue architecture of the wing without changing genetic background, and does not adversely affect normal developmental timing. Although it remains to be addressed how Dpp ligands move between dorsal and ventral cells, our observations suggest that the basolateral polarity determinant Scribble (Scrib) may be involved in interplanar signaling (*SI Appendix*, Fig. S7 *A* and *B*). Since previous studies showed that Scrib mediates a positive feedback mechanism between BMP signaling and wing vein morphogenesis in the posterior crossvein region of the pupal wing (34), the polarization of epithelial cells may play a role in interplanar signaling. Taken together, we propose that pupal wing morphogenesis and Dpp signaling are coupled, and 3D tissue architecture plays an instructive role in regulating the spatiotemporal distributions of Dpp signaling.

We suspect that mechanisms similar to those found in this study may play roles in the development of many organs and tissues across species. Communication between apposed tissues is likely to be crucial for many developmental processes, but has been insufficiently studied to date. Do cells secrete extrinsic factors to aid the opposing tissues in finding each other across an open space? Is tight coordination of cell proliferation a key process in correct alignment of apposing tissues? If these are the case, what triggers the cellular responses that arise before the tissues come into contact?

In mammalian embryo development, there are many instances when two apposing tissues approach one another and fuse to form a continuous tissue. This type of process is crucial for the correct formation and functions of many organs and tissues, including the face, neural tube and eyes (35–38). Disruption of fusion leads to various birth defects, including cleft palate, neural tube defects and disorders of eyelid formation (39–41). Although the molecular mechanisms of tissue fusion are likely to be context-dependent, many of the tissue fusion events may share similar mechanisms. Before fusion, cellular events such as cell proliferation, apoptosis, migration and epithelial-mesenchymal transition must be coordinated in space and time.

One of the best characterized systems of tissue fusion is the palate, the tissue that separates the oral cavity from the nasal cavity and forms the roof of the mouth. During mammalian embryogenesis, palatogenesis is regulated by a network of signaling molecules and transcription factors to tightly regulate

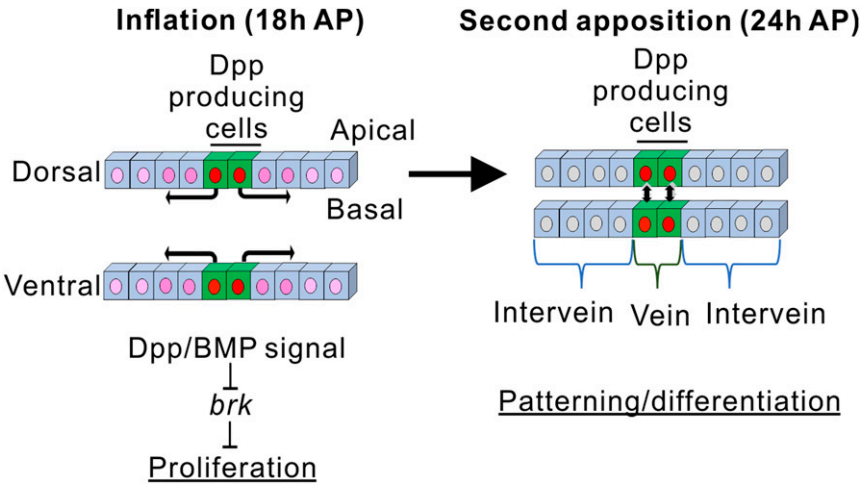

Fig. 7. Schematics of coupling between 3D tissue architecture and Dpp signaling. During the inflation stage, Dpp expressed in the longitudinal vein primordia cells diffuses laterally and inhibits *brk* expression to regulate tissue proliferation. After reapposition, Dpp signaling actively takes place between dorsal and ventral cells to refine signaling range for vein patterning/differentiation.

cellular processes (36, 42). Many studies, in both humans and mice, have identified transforming growth factor (TGF)-β3 as a key signaling factor regulating palate fusion (43–45). Mice deficient in TGF-β3 show fully penetrant cleft palate phenotypes, providing an animal model with which to study TGF-β3 function in palatal fusion (43). TGF-β3 is expressed in the medial edge epithelial cells before adhesion of the opposing palatal shelves, and continues to be expressed during palatal fusion (46). By using a method of palatal shelf organ culture, Taya et al. (47) demonstrated that coculture of a TGF-β3 null mutant palatal shelf with wild type palatal shelf resulted in fusion. This result suggested that TGF-β3 produced in wild-type palatal shelf diffused across and rescued the TGF-β3 mutant shelf, allowing fusion.

Furthermore, it is likely that organogenesis from stem cells and tissue self-organization require related mechanisms (48, 49). Characterizing coupling mechanisms between extrinsic signals and morphological changes may therefore further enhance our understanding of organogenesis and morphogenesis.

In summary, our data provide novel insights into how dynamics of 3D tissue architecture instruct spatiotemporal regulation of BMP signaling. We surmise that the concepts highlighted in this work may be generally applicable to molecular mechanisms of animal development, as well as organogenesis from stem cells.

Materials and Methods

Fly Genetics. *nub-GAL4* (#25754), *ap-GAL4* (#3041), *tubP-GAL80^{ts}* (#7017), w; *UAS-GFP-dpp* (#53716) *w*; *His2Av-RFP* (#23650), *w*;; *His2Av-RFP* (#23651), and *scrib^{2}* (#41775) were obtained from the Bloomington *Drosophila* Stock Center. *UAS-tkv* RNAi (#3059) was obtained from the Vienna *Drosophila* RNAi Center. *Tkv-YFP^{CPTI00248}* (#115298) was obtained from the Kyoto *Drosophila* Genetic Resources Center. *dpp$^{FRT.CA}$*; *rn-Gal4 and dpp$^{FRT.CA}$*, *UAS-Flp were obtained from* JP Vincent, *dpp^{FO}*; *UAS-FLP*, *dpp^{FO} nub-GAL4*, and *dpp^{FO} ap-Gal4* (the *dpp^{FO}*, referred as *dpp^{TA}* in this paper) from M. Gibson, *w*, *αTubulin-GFP from* C. Gonzalez, *UAS-Dad* from T. Tabata, and *brk^{B14F}-GFP and UAS-brk* from G. Pyrowolakis. Fly stocks were maintained at 25 °C unless otherwise mentioned.

To generate the *dpp^{FO}* mutant, mid-third instar larvae, raised at 18 °C for 7–8 d after egg laying (AEL), were shifted to 29 °C for 8 h (*dpp$^{FRT.CA}$*) (9) or 24 h before pupariation (*dpp$^{FRT.TA}$*) (8). Late-third instar larvae and white prepupae were subjected to the subsequent experiments, including immunostaining and in situ hybridization.

For exogenous expression of *Dad* or shRNA at pupal stages, white prepupae raised at 18 °C or room temperature were shifted to 29 °C, and the pupae of indicated ages were collected and subjected to the subsequent experiments.

For MARCM analysis, flies were maintained at 25 °C throughout development, except for heat-shock treatment. Three days AEL, second instar larvae underwent heat shock for 2 h in a 37 °C water bath. Thereafter, white prepupae were collected, and those aged to 24 h were fixed and subjected to immunostaining analysis.

Pupal wings were dissected at developmental timepoints equivalent to 25 °C. Calculations for developmental timing at 29 °C were based on previously published data (50).

Full Genotypes. Fig. 1 *B–D*: *w*; *dpp$^{FRT.CA}$*, *UAS-Flp/+*; *rn-Gal4/tubP-Gal80^{ts}*
Fig. 1 *E–G*: *w*; *dpp$^{FRT.CA}$*, *UAS-Flp/dpp$^{FRT.CA}$*; *rn-Gal4/tubP-Gal80^{ts}*
Figs. 2 *A–E* and 6*B*: *brk^{B14F}-GFP* (III)
Fig. 2*G*: *w*; *nub-Gal4/dpp$^{FRT.TA}$*; *UAS-Flp/tubP-Gal80^{ts}*
Fig. 2*H*: *w*; *dpp$^{FRT.TA}$*, *nub-Gal4/dpp$^{FRT.TA}$*; *UAS-Flp/tubP-Gal80^{ts}*
Figs. 2 *K–N* and 6*C*: *w*; *Tkv-YFP^{CPTI00248}/+*
Figs. 2 *P* and *Q* and 6 *E* and *F*: *w*; *dpp$^{FRT.CA}$/+*
Fig. 2*R*: *w*; *nub-Gal4/UAS-brk*; *tubP-Gal80^{ts}/+*
Fig. 2*S*: *w*; *nub-Gal4/+*; *tubP-Gal80^{ts}/+*
Fig. 3 *A–E*: *w*, *ubi-αTubulin:GFP*
Fig. 3*G*: *ap-Gal4/+*; *tubP-Gal80^{ts}/+*
Fig. 3*H*: *w*; *ap-Gal4/UAS-Dad*; *tubP-Gal80^{ts}/+*
Fig. 3*I*: *w*; *ap-Gal4/UAS-tkv^{RNAi}*; *tubP-Gal80^{ts}/+*
Fig. 3*J*: *ap-Gal4/+*; *tubP-Gal80^{ts} brk^{B14F}-GFP/+*
Fig. 3*K*: *w*; *ap-Gal4/UAS-Dad*; *tubP-Gal80^{ts} brk^{B14F}-GFP/+*
Fig. 3*L*: *w*; *ap-Gal4/UAS-tkv^{RNAi}*; *tubP-Gal80^{ts} brk^{B14F}-GFP/+*
Fig. 3 *N*, *O*, and *Q*: *w*; *dpp$^{FRT.TA}$*, *ap-Gal4/dpp$^{FRT.TA}$*; *UAS-Flp/tubP-Gal80^{ts}*
Fig. 3*P*: *w*; *ap-Gal4/dpp$^{FRT.TA}$*; *UAS-Flp/tubP-Gal80^{ts}*
Fig. 4 *A–D*: *hs-Flp*; *tubP-Gal4 UAS-mCD8-GFP/UAS-GFP-dpp*; *tubP-Gal80^{ts} FRT^{82B}/FRT^{82B}*
Fig. 5 *A–F*: *w*; *+/UAS-Dad*; *His2Av-RFP/brk^{B14F}-GFP*, *tubP-Gal80^{ts}*
Fig. 5 *G–L*: *w*; *ap-Gal4/UAS-Dad*; *His2Av-RFP/brk^{B14F}-GFP*, *tubP-Gal80^{ts}*
SI Appendix, Fig. S1 *A* and *F–H*: *w*; *dpp$^{FRT.TA}$*, *nub-Gal4/dpp$^{FRT.TA}$*; *UAS-Flp/tubP-Gal80^{ts}*
SI Appendix, Fig. S1 *B–E*: *w*; *nub-Gal4/dpp$^{FRT.TA}$*; *UAS-Flp/tubP-Gal80^{ts}*
SI Appendix, Fig. S1 *L* and *M*: *w*; *nub-Gal4/+*; *tubP-Gal80^{ts}/+*
SI Appendix, Fig. S1 *N* and *O*: *w*; *nub-Gal4/UAS-Dad*; *tubP-Gal80^{ts}/+*
SI Appendix, Fig. S2 *A–D*: *yw*
SI Appendix, Fig. S2*E*: *w*; *nub-Gal4/UAS-Dad*; *tubP-Gal80^{ts}/brk^{B14F}-GFP*
SI Appendix, Fig. S3 *A–C*: *w*; *ap-Gal4/dpp$^{FRT.TA}$*; *UAS-Flp/tubP-Gal80^{ts}*
SI Appendix, Fig. S3*D*: *w*; *dpp$^{FRT.TA}$*, *ap-Gal4/dpp$^{FRT.TA}$*; *UAS-Flp/tubP-Gal80^{ts}*
SI Appendix, Fig. S4 *A* and *B*: *hs-Flp*; *tubP-Gal4 UAS-mCD8-GFP/UAS-GFP-dpp*; *tubP-Gal80^{ts} FRT^{82B}/FRT^{82B}*
Fig. 4 *C* and *D*: *hs-Flp tubP-Gal80 FRT^{19A}/FRT^{19A}*; *tubP-Gal4 UAS-mCD8-GFP/UAS-Dad*; *UAS-GFP-dpp/+*
SI Appendix, Fig. S5 *A–F*: *w*; *+/UAS-Dad*; *His2Av-RFP/brk^{B14F}-GFP*, *tubP-Gal80^{ts}*
SI Appendix, Fig. S5 *G–L*: *w*; *ap-Gal4/UAS-Dad*; *His2Av-RFP/brk^{B14F}-GFP*, *tubP-Gal80^{ts}*
SI Appendix, Fig. S6: *Oregon R*
SI Appendix, Fig. S7 *A* and *B*: *hs-Flp*; *tubP-Gal4 UAS-mCD8-GFP/UAS-GFP-dpp*; *tubP-Gal80^{ts} FRT^{82B}/FRT^{82B} scrib^{2}*

Immunohistochemistry. Pupae were fixed in 3.7% formaldehyde (Sigma-Aldrich) at 4 °C overnight, after which pupal wings were dissected. Larvae were fixed in 3.7% formaldehyde at room temperature for 20 min, after which wing imaginal discs were dissected. The following primary antibodies were used: mouse anti-DLG1 [1:50; Developmental Studies Hybridoma Bank (DSHB), University of Iowa], rabbit anti-phospho-SMAD1/5 (1:300; Cell Signaling Technologies), rabbit anti-phospho-Histone H3 (1:500; Millipore), rat anti-HA 3F10 (1:100; Roche). Alexa 488 conjugated phalloidin (1:200; Thermo Fisher Scientific). Secondary antibodies were anti-mouse IgG Alexa 488, anti-rabbit IgG Alexa 568, anti-mouse IgG Alexa 647, and-rat IgG Alexa 568 (1:200; Thermo Fisher Scientific).

Imaging and Image Analysis. Fluorescent images were obtained with a Zeiss LSM700 upright laser confocal microscope, in situ hybridization images and adult wing images were obtained with a Nikon ECLIPSE 90i microscope. All images were processed and analyzed with ImageJ (NIH) software. Images subjected to intensity measurement were captured with the same parameters, otherwise, the images were adjusted with linear methods. The "remove outliner" function of ImageJ was applied to remove bright speckles, which are nonspecific signal, in some images. None of the processing steps affect data interpretation.

Time Lapse Imaging. Prepupae of indicated genotypes were raised and collected at room temperature, then shifted to 29 °C until staged appropriately (late inflation stage, roughly 18 h AP equivalent at 25 °C). Pupae were retrieved, briefly rinsed in water, dried on a Kimwipe, then positioned on a piece of double-sided tape (right wing facing up). Windows were carefully dissected into the pupal cases in the region of the wing using a microknife (cat# 10316–14; Fine Science Tools) essentially as described (51), avoiding damage to the underlying tissue. A tiny drop of halocarbon oil (Sigma Aldrich) was applied to the exposed pupal wing with a disposable pipet tip to prevent tissue desiccation during imaging. The pupae, adhering to strips of double-sided tape cut with a disposable scalpel, were then placed oil-side down onto a 24 × 50 mm coverslip. After 5–6 pupae were collected onto the coverslip, wings were time-lapse imaged on a Leica SP8 STED confocal microscope by taking optical anteroposterior cross sections of each wing every 4–5 min using the xzyt-function. The resulting time lapse images were processed into AVI-format videos using Imaris v.9.1.2 (Bitplane/Oxford Instruments).

Modulation of Tissue Architecture of the Pupal Wings Through Abdominal Squeezing. Pupal cases of 18 h AP pupae were carefully removed from the anterior to expose the wings. Then, the pupae were positioned with dorsal side facing up before forceps were used to clasp the abdomen. Once the abdomen was stabilized, we exerted force by gently squeezing the abdomen with the forceps. The force was gradually increased until influx of hemolymph into the wings was observed, which causes the enhanced inflation. After squeezing, the pupae were maintained at 25 °C in a humid chamber and subjected to the experiments at the indicated time points.

Statistics. All experiments were carried out independently at least three times. Data are means ±95% confidence intervals (CIs). Statistical significance was calculated by the two paired *t* test method.

ACKNOWLEDGMENTS. We thank Jukka Jernvall and Irma Thesleff for thoughtful comments on the manuscript. We thank M. Gibson, J. P. Vincent, T. Tabata, C. Gonzalez, and G. Pyrowolakis for fly stocks. This work was supported by Grant 265648, 308045 from the Academy of Finland, the Sigrid Juselius Foundation, and the Center of Excellence in Experimental and Computational Developmental Biology from the Academy of Finland (to O.S.), Grant 295013 from the Academy of Finland (to D.T.-M.), JSPS KAKENHI (Grants-in-Aid for Scientific Research) Grants 7K00410 and 17KK0007 (to Y.I.), the Integrative Life Science Doctoral Program of the University of Helsinki (J.G.), and the Finnish Cultural Foundation (Y.H.).

1. Gilmour D, Rembold M, Leptin M (2017) From morphogen to morphogenesis and back. *Nature* 541:311–320.
2. Durdu S, et al. (2014) Luminal signalling links cell communication to tissue architecture during organogenesis. *Nature* 515:120–124.
3. Shyer AE, Huycke TR, Lee C, Mahadevan L, Tabin CJ (2015) Bending gradients: How the intestinal stem cell gets its home. *Cell* 161:569–580.
4. Matsuda S, Blanco J, Shimmi O (2013) A feed-forward loop coupling extracellular BMP transport and morphogenesis in Drosophila wing. *PLoS Genet* 9:e1003403.
5. Shimmi O, Newfeld SJ (2013) New insights into extracellular and post-translational regulation of TGF-β family signalling pathways. *J Biochem* 154:11–19.
6. Affolter M, Basler K (2007) The decapentaplegic morphogen gradient: From pattern formation to growth regulation. *Nat Rev Genet* 8:663–674.
7. Restrepo S, Zartman JJ, Basler K (2014) Coordination of patterning and growth by the morphogen DPP. *Curr Biol* 24:R245–R255.
8. Akiyama T, Gibson MC (2015) Decapentaplegic and growth control in the developing Drosophila wing. *Nature* 527:375–378.
9. Bosch PS, Ziukaite R, Alexandre C, Basler K, Vincent JP (2017) Dpp controls growth and patterning in Drosophila wing precursors through distinct modes of action. *eLife* 6: e22546.
10. Blair SS (2007) Wing vein patterning in Drosophila and the analysis of intercellular signaling. *Annu Rev Cell Dev Biol* 23:293–319.
11. Matamoro-Vidal A, Salazar-Ciudad I, Houle D (2015) Making quantitative morphological variation from basic developmental processes: Where are we? The case of the Drosophila wing. *Dev Dyn* 244:1058–1073.
12. Pastor-Pareja JC, Grawe F, Martín-Blanco E, García-Bellido A (2004) Invasive cell behavior during Drosophila imaginal disc eversion is mediated by the JNK signaling cascade. *Dev Cell* 7:387–399.
13. Aldaz S, Escudero LM, Freeman M (2010) Live imaging of Drosophila imaginal disc development. *Proc Natl Acad Sci USA* 107:14217–14222.
14. Waddington CH (1940) The genetic control of wing development in Drosophila. *J Genet* 41:75–139.
15. Fristrom D, Wilcox M, Fristrom J (1993) The distribution of PS integrins, laminin A and F-actin during key stages in Drosophila wing development. *Development* 117: 509–523.
16. Segal D, Gelbart WM (1985) Shortvein, a new component of the decapentaplegic gene complex in Drosophila melanogaster. *Genetics* 109:119–143.
17. St Johnston RD, et al. (1990) Molecular organization of the decapentaplegic gene in Drosophila melanogaster. *Genes Dev* 4:1114–1127.
18. Tsuneizumi K, et al. (1997) Daughters against Dpp modulates Dpp organizing activity in Drosophila wing development. *Nature* 389:627–631.
19. Etournay R, et al. (2016) TissueMiner: A multiscale analysis toolkit to quantify how cellular processes create tissue dynamics. *eLife* 5:e14334.
20. Milán M, Campuzano S, García-Bellido A (1996) Cell cycling and patterned cell proliferation in the Drosophila wing during metamorphosis. *Proc Natl Acad Sci USA* 93: 11687–11692.
21. O'Keefe DD, et al. (2012) Combinatorial control of temporal gene expression in the Drosophila wing by enhancers and core promoters. *BMC Genomics* 13:498.
22. Schubiger M, Palka J (1987) Changing spatial patterns of DNA replication in the developing wing of Drosophila. *Dev Biol* 123:145–153.
23. Matsuda S, Shimmi O (2012) Directional transport and active retention of Dpp/BMP create wing vein patterns in Drosophila. *Dev Biol* 366:153–162.
24. Müller B, Hartmann B, Pyrowolakis G, Affolter M, Basler K (2003) Conversion of an extracellular Dpp/BMP morphogen gradient into an inverse transcriptional gradient. *Cell* 113:221–233.
25. Campbell G, Tomlinson A (1999) Transducing the Dpp morphogen gradient in the wing of Drosophila: Regulation of Dpp targets by brinker. *Cell* 96:553–562.
26. Gafner L, et al. (2013) Manipulating the sensitivity of signal-induced repression: Quantification and consequences of altered brinker gradients. *PLoS One* 8:e71224.
27. Minami M, Kinoshita N, Kamoshida Y, Tanimoto H, Tabata T (1999) Brinker is a target of Dpp in Drosophila that negatively regulates Dpp-dependent genes. *Nature* 398: 242–246.
28. Schwank G, Restrepo S, Basler K (2008) Growth regulation by Dpp: An essential role for brinker and a non-essential role for graded signaling levels. *Development* 135: 4003–4013.
29. Martín FA, Pérez-Garijo A, Moreno E, Morata G (2004) The brinker gradient controls wing growth in Drosophila. *Development* 131:4921–4930.
30. Lee T, Luo L (1999) Mosaic analysis with a repressible cell marker for studies of gene function in neuronal morphogenesis. *Neuron* 22:451–461.
31. Schuh M, Lehner CF, Heidmann S (2007) Incorporation of Drosophila CID/CENP-A and CENP-C into centromeres during early embryonic anaphase. *Curr Biol* 17:237–243.
32. Lecuit T, Cohen SM (1998) Dpp receptor levels contribute to shaping the Dpp morphogen gradient in the Drosophila wing imaginal disc. *Development* 125:4901–4907.
33. García-Bellido A (1977) Inductive mechanisms in the process of wing vein formation inDrosophila. *Wilehm Roux Arch Dev Biol* 182:93–106.
34. Gui J, Huang Y, Shimmi O (2016) Scribbled optimizes BMP signaling through its receptor internalization to the Rab5 endosome and promote robust epithelial morphogenesis. *PLoS Genet* 12:e1006424.
35. Ray HJ, Niswander L (2012) Mechanisms of tissue fusion during development. *Development* 139:1701–1711.
36. Bush JO, Jiang R (2012) Palatogenesis: Morphogenetic and molecular mechanisms of secondary palate development. *Development* 139:231–243.
37. Nikolopoulou E, Galea GL, Rolo A, Greene ND, Copp AJ (2017) Neural tube closure: Cellular, molecular and biomechanical mechanisms. *Development* 144:552–566.
38. Rubinstein TJ, Weber AC, Traboulsi EI (2016) Molecular biology and genetics of embryonic eyelid development. *Ophthalmic Genet* 37:252–259.
39. Dixon MJ, Marazita ML, Beaty TH, Murray JC (2011) Cleft lip and palate: Understanding genetic and environmental influences. *Nat Rev Genet* 12:167–178.
40. Greene ND, Copp AJ (2014) Neural tube defects. *Annu Rev Neurosci* 37:221–242.
41. Tao H, et al. (2005) A dual role of FGF10 in proliferation and coordinated migration of epithelial leading edge cells during mouse eyelid development. *Development* 132: 3217–3230.
42. Smith TM, Lozanoff S, Iyyanar PP, Nazarali AJ (2013) Molecular signaling along the anterior-posterior axis of early palate development. *Front Physiol* 3:488.
43. Proetzel G, et al. (1995) Transforming growth factor-beta 3 is required for secondary palate fusion. *Nat Genet* 11:409–414.
44. Kaartinen V, et al. (1995) Abnormal lung development and cleft palate in mice lacking TGF-beta 3 indicates defects of epithelial-mesenchymal interaction. *Nat Genet* 11:415–421.
45. Iwata J, Parada C, Chai Y (2011) The mechanism of TGF-β signaling during palate development. *Oral Dis* 17:733–744.
46. Yang LT, Kaartinen V (2007) Tgfb1 expressed in the Tgfb3 locus partially rescues the cleft palate phenotype of Tgfb3 null mutants. *Dev Biol* 312:384–395.
47. Taya Y, O'Kane S, Ferguson MW (1999) Pathogenesis of cleft palate in TGF-beta3 knockout mice. *Development* 126:3869–3879.
48. Lancaster MA, Knoblich JA (2014) Organogenesis in a dish: Modeling development and disease using organoid technologies. *Science* 345:1247125.
49. Sasai Y (2013) Cytosystems dynamics in self-organization of tissue architecture. *Nature* 493:318–326.
50. Buttitta LA, Katzaroff AJ, Perez CL, de la Cruz A, Edgar BA (2007) A double-assurance mechanism controls cell cycle exit upon terminal differentiation in Drosophila. *Dev Cell* 12:631–643.
51. Classen AK, Aigouy B, Giangrande A, Eaton S (2008) Imaging Drosophila pupal wing morphogenesis. *Methods Mol Biol* 420:265–275.